e-ISSN 2621-9883
Elipsoida : Jurnal Geodesi dan Geomatika
Vol 08 No 02, (2025)

COMPARATIVE STUDY OF LAND SURFACE TEMPERATURE ON LANDSAT 8 AND HLS-L30 USING MONO WINDOW AND SPLIT WINDOW ALGORITHMS (CASE STUDY: WKP MOUNT UNGARAN)

Yolanda Stevany Nababan*, Rizki Amara Putri, Nurhadi Bashit, Firman Hadi, Taufiq Ihsanudin
[1234]Department of Geodetic Engineering, Diponegoro University, Semarang, Indonesia
[5]Sekolah Tinggi Pertanahan Nasional (STPN), Yogyakarta, Indonesia
Corresponding author(s) e-mail: yolandastevany9@gmail.com*

(Received 25 July 2025, Accepted 26 November 2025, Published 04 December 2025)

ABSTRACT

Advancements in remote sensing technology have enabled the use of satellite imagery, such as Landsat 8 and HLS-L30, for the spatial and temporal estimation of Land Surface Temperature (LST) with improved resolution. In the context of geothermal exploration, the availability of thermal infrared bands in these datasets facilitates more efficient and cost-effective mapping and identification of surface temperature anomalies, particularly across large and inaccessible areas. This study aims to compare LST estimations derived from Landsat 8 and HLS-L30 imagery using the Mono Window Algorithm (MWA) and Split Window Algorithm (SWA) at 18 geothermal manifestation points within the Mount Ungaran Geothermal Working Area (WKP). A Focal Statistic process was applied to 20 LST datasets, resulting in a total of 100 LST layers. From each layer, LST values were extracted at the 18 manifestation points, producing a total of 1,800 data points. A binary logistic regression analysis was conducted using these LST values alongside those from 20 randomly selected comparison points. The results indicate that the median LST derived from HLS-L30 imagery using the Split Window Algorithm with the minimum Focal Statistic yielded the most optimal performance in classifying geothermal manifestation presence. This method achieved statistical significance ($p = 0.028$), indicating its capability to effectively distinguish between manifestation and non-manifestation points. However, the pseudo-R^2 value of 0.107 suggests that the model explains approximately 11% of the variance in the data. These findings underscore the potential application of satellite-based LST analysis in the early detection and assessment of geothermal surface anomalies within WKPs.

Keywords : HLS-L30, Geothermal, Landsat, LST, Ungaran

1. INTRODUCTION

Indonesia has geothermal potential spread along volcanic lines amounting to 29 Gigawatts (GW) or about 40% of the world's total potential (Kementerian Energi dan Sumber Daya Mineral, 2013). Based on data from (Pambudi et al., 2024) the installed geothermal generation capacity in the world reached 16,127 MW of which 2,356 MW was installed in Indonesia. Thus, Indonesia has only utilized less than 10% of the total potential. One of the regions in Indonesia that has geothermal potential is Central Java Province. According to data from (Dinas Energi dan Sumber Daya Mineral Provinsi Jawa Tengah, 2022) the geothermal potential in Central Java reaches 969 Mwe spread across six Geothermal Working Areas (WKP), one of which is the WKP Mount Ungaran. The existence of manifestations such as hot springs and cold springs is an indication of geothermal potential in this region.

Early identification of geothermal prospective zones in an area is an important step in the geothermal energy exploration process (Ramadhan & Saputra, 2021). One of the parameters that play an important role in this process is the land surface temperature (LST) because it can reflect the estimation and heat anomalies that are directly related to geothermal activity in the subsurface. The results of research by (Akhyar & Sary, 2024) confirmed that in Mount Seulawah, areas that have high LST values can be estimated as areas that have anomalies and can be used to identify geothermal prospective zones. Along with the development of remote sensing technology, LST estimation from satellite imagery is an alternative in geothermal monitoring, especially in areas that are difficult to access (Ramadhani & Hidayat, 2021).

Landsat 8 and Harmonized Landsat-Sentinel (HLS-L30) are two medium-resolution satellite data sources that can be used in LST estimation because they provide spatially and temporally consistent thermal channels and surface reflectance (Ju et al., 2023) (Engebretson, 2020). Many studies have utilized the thermal channel of Landsat 8 satellite

imagery in processing LST estimation in a geothermal manifestation. Geothermal research around the Mount Ungaran area conducted by (Izzatinavia et al., 2024) used Landsat 8 channel 10 to estimate LST. The LST results in this study revealed that subsurface geothermal manifestations such as hot springs, fumaroles, or hot steam, usually originate from geothermal systems in the ground. Such geothermal manifestations may indicate the presence of geothermal anomalies that could affect the LST in the region. Another study conducted by (Mirwanda et al., 2021) utilized Landsat 8 channel 10 with the Mono Window algorithm method to map surface temperature anomalies in the Mount Ciremai area which resulted in a temperature range of 15-31°C. The LST anomaly is mapped at the top of Mount Ciremai which is the location of the crater and in the northeast to southeast of the top of Mount Ciremai. In addition, research (Utama et al., 2024) used Landsat 8 to map LST and NDVI, and found that geothermal manifestation points on Mount Lawu are in sparsely to moderately vegetated areas with relatively high LST.

Therefore, early estimation of temperature in geothermal potential areas is still very possible with remote sensing satellite imagery. Although there have been studies that examine the utilization of LST in the context of geothermal, there has been no comparative study between LST from Landsat 8 and HLS-L30 on geothermal manifestation points in Indonesia.

This research aims to conduct a comparative study of LST estimation from Landsat 8 and HLS-L30 on geothermal manifestation points in WKP Mount Ungaran. LST estimation uses two methods, namely Mono Window Algorithm (MWA) and Split Window Algorithm (SWA). The LST results were analyzed statistically to evaluate the distribution and homogeneity of the data and a binary (dichotomous) logistic regression model was used to test the ability of LST to distinguish between 18 geothermal manifestation points (combined hot and cold springs) and 20 random sample points that have no indication of geothermal. The results of this study are expected to be a reference in the selection of the right type of data and LST estimation method to support remote sensing-based geothermal energy early exploration activities, especially in the WKP Mount Ungaran.

2. DATA AND METHODOLOGY

2.1 Location and Data of Research

2.1.1 Research Location

Mount Ungaran is one of the mountains in Central Java, precisely located at latitude 7°07'42.69" – 7°15'44.96" S dan 110°18'42.36" – 110°29'35.16" E (Kementerian Energi dan Sumber Daya Mineral Republik Indonesia, 2007). The location of this research is in WKP Mount Ungaran which can be seen in **Figure 1**.

Mount Ungaran is located in the back arc zone with an altitude of approximately 2050 meters above sea level. The WKP Mount Ungaran is located 40 km to the southwest of Semarang Regency. Geothermal indications in this area are characterized by the appearance of several manifestations, namely fumaroles and hot springs. The geothermal potential in Ungaran is in the Gedongsongo area with an estimated potential reserve of 100 MW.

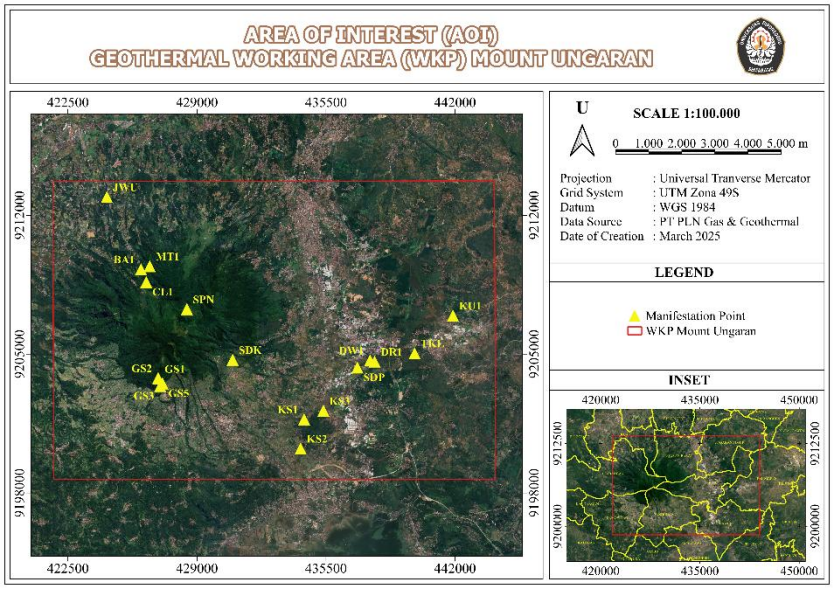

Figure 1. WKP Mount Ungaran

2.1.2 Research Data

In this study, the data collection period of the three images, namely Landsat 8 OLI/TIRS collection 2 digital number, Landsat 8 OLI-TIRS collection 2 surface reflectance, and HLS operational land imager surface reflectance and toa brightness daily global 30 m (HLS-L30) was carried out throughout 2019 with the provision of cloud cover> 10% in the AOI region. While MODIS (MYD05 Level 2) follows the acquisition date of the Landsat 8 OLI/TIRS collection 2 digital number and HLS-L30 image because it is for data extraction of the amount of water vapor that will be used in the LST estimation process using the Split Window method. Complete information about the data used can be seen in **Table 1**.

Table 1. Research Data

Feature	Data Type	Acquisition Date	Data Source	Application
Landsat 8 OLI/TIRS collection 2 digital number	Raster	2019	Google Earth Engine (GEE)	Mono Window Algorithm (MWA) and Split Window Algorithm (SWA) LST processing
Landsat 8 OLI-TIRS collection 2 surface reflectance	Raster	2019	Google Earth Engine (GEE)	Mono Window Algorithm (MWA) LST processing
MODIS (MYD05 Level 2)	Raster	2019	NASA	Extraction of data on the total amount of water vapor in the atmosphere (Precipitable Water Vapor) using the near-infrared (NIR) band.
HLS operational land imager surface reflectance and toa brightness daily global 30 m (HLS-L30)	Raster	2019	Google Earth Engine (GEE)	Mono Window Algorithm (MWA) and Split Window Algorithm (SWA) LST processing
Geothermal manifestation points	Vector	2019	PT PLN Gas & Geothermal	Information on 18 manifestation points and surface temperature in the process of normality test, homogeneity test, and binary logistic regression test.
20 random sample points	Vector	September 2019	Digitized on screen (random sampling method)	Additional data for binary logistic regression test for each LST data.

2.2 Methodology

In this research, Landsat 8 Operational Land Imager (OLI) - Thermal Infrared Sensor (TIRS) Collection 2 Digital Number and Surface Reflectance and HLS-L30, with the provision of maximum cloud cover in the AOI region of 10%, will be imported using Google Earth Engine (GEE) to calculate LST. While the MODIS (MYD05 Level 2) near-infrared (NIR) channel is imported from the NASA website for the extraction of water vapor content. The flowchart of this research can be seen in **Figure 2**.

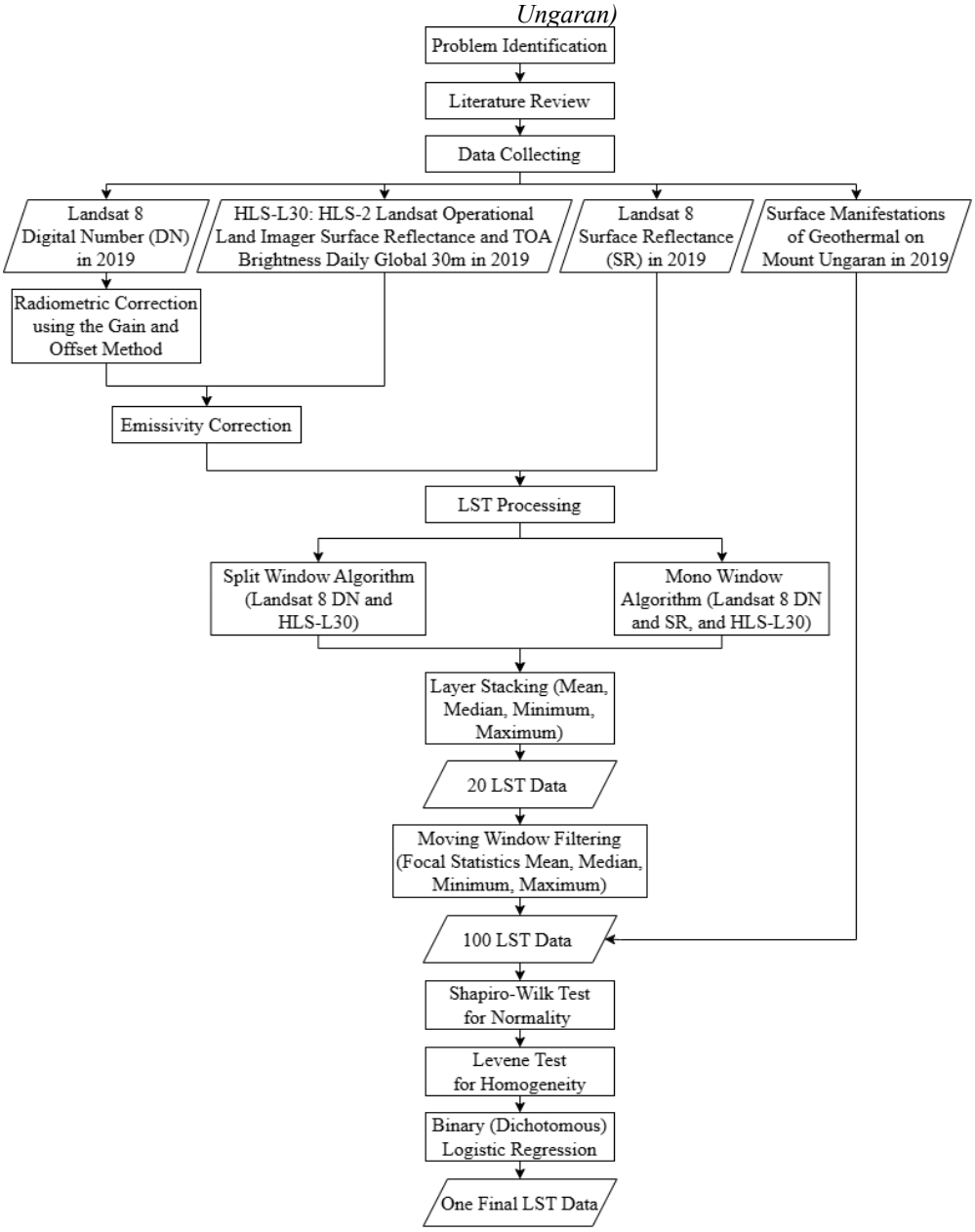

Figure 2. Research Flowchart

2.2.1 HLS-L30

The Harmonized Landsat and Sentinel-2 (HLS) project is a NASA initiative and collaboration with the USGS to produce compatible surface reflectance (SR) data from a virtual constellation of satellite sensors, namely the Operational Land Imager (OLI) and Multi-Spectral Instrument (MSI) on board the Landsat-8 and Sentinel-2 remote sensing satellites (Ju et al., 2023). he HLS suite consists of two products, S30 and L30, derived from Sentinel-2 L1C and Landsat L1TP input data (Collection 2). The L30 product contains Landsat-8 OLI surface reflectance and TOA TIRS brightness temperature gridded at 30 m spatial resolution in MGRS tiles.

2.2.2 Data Pre-Processing

A. Radiometric Correction Gain and Offset Method

This correction aims to convert data in the image in the form of digital number (DN) into radiance or reflectance. The data needed is radiance or reflectance multiple rescalling factor (GAIN) and additive rescalling factor (OFFSET).

1) DN to TOA Reflectance (ρ) Conversion

The DN to reflectance conversion uses the following formula (Landsat Missions, 1984).

$$\rho\lambda' = M\rho Qcal + A\rho \quad \text{.....(1)}$$

Description:
- $\rho\lambda'$: TOA Spectral Reflectance
- ρM : Rescalling factor value from the metadata
- ρA : Rescalling factor value from the metadata

2) DN to TOA Radiance (L) Conversion

Landsat 8 Digital Number can be converted to TOA radiance using the following formula (Landsat Missions, 1984).

$$L\lambda = MlQcal + Al \quad \text{.....(2)}$$

Description:
- $L\lambda$: TOA spectral radiance
- Ml : Canal-specific multiplicative rescalling factor from metadata
- Al : Canal-specific additive rescalling factor from metadata
- $Qcal$: Canal to be radiometrically corrected

B. Radiometric Correction Brightness Temperature Method

This method is used to convert ToA radiance into brightness temperature using the formula (Yanis et al., 2023):

$$BT = \frac{K2}{\{ln(\frac{K1}{L\lambda}+1)\}} - 273 \quad \text{.....(3)}$$

Description:
- BT : Brightness Temperature (°C)
- $L\lambda$: TOA spectral radiance
- K1 : Band-specific thermal conversion constant from the metadata (K1_CONSTANT_BAND_x, where x is the band number, 10 or 11)
- K2 : Band-specific thermal conversion constant from the metadata (K2_CONSTANT_BAND_x, where x is the band number, 10 or 11)

2.2.3 Land Surface Temperature Estimation

The LST calculation method was carried out using two methods, namely Mono Window Algorithm (MWA) and Split Window Algorithm (SWA).

A. Mono Window Algorithm (MWA)

The MWA LST formula was used from the formula developed by (Yanis et al., 2023). The MWA formula connects the thermal brightness (BT) value in channel 10 of the satellite image and the proportion of vegetation (PV) obtained through NDVI.

$$PV = \frac{(NDVI - NDVI_{min})}{(NDVI_{max} + NDVI_{min})} \quad \text{..... (4)}$$

Description:
- NDVI : Vegetation index processing results
- $NDVI_{min}$: Minimum value of vegetation index processing results
- $NDVI_{max}$: Maximum value of vegetation index processing results

The PV value above is used to calculate the Land Surface Emissivity value using the following formula.

$$E = 0.004 \times PV + 0.986 \quad \text{..... (5)}$$

Description:
- 0.004 : Average emissivity value of dense vegetation
- 0.986 : Standard emissivity value of open land
- PV : Vegetation Proportion Value

The BT, PV, and E values are used to calculate the LST value through equation (Yanis et al., 2023) as shown below.

$$LST = \frac{BT}{\left[1 + \left(\left(\lambda \, x \frac{BT}{\rho}\right) x \, ln(E)\right)\right]} \quad \text{..... (6)}$$

Description:
- BT : Brightness Temperature (°C)
- λ : Band 10 average wavelength
- PV : Vegetation Proportion Value
- E : Emissivity value
- P = (h*c/s) of 14,380 mK
- C = Speed of light 3 x 10^8 m/s
- S = Bolztmann's constant of 1.38 x 10^{-23}J/K

B. Split Window Algorithm (SWA)

In the process of obtaining the estimated land surface temperature (LST) using the SWA method, researchers used an empirical formula developed by (Sobrino et al., 2001). The SWA LST equation connects the brightness value (BT) in channel 10 with channel 11 of the satellite image. The surface emissivity value obtained from the calculation of the FVC proportion.

$$FVC = \frac{(NDVI - NDVI_{soil})}{(NDVI_{veg} + NDVI_{soil})} \quad \text{..... (7)}$$

Keterangan:
- FVC = Fractional Vegetation Cover
- NDVI = Vegetation index processing result
- $NDVI_{soil}$: NDVI value for soil = 0.2
- $NDVI_{veg}$: NDVI value for vegetation = 0.9

The PVC value is used to calculate the LSE value through the following formula.

$$LSE = E_s \times (1 - FVC) + E_V \times FVC \quad \text{.....(8)}$$

Description:
LSE : Land Surface Emissivity
E_S : Soil Emissivity Value
E_V : Vegetation Emissivity Value
FVC : Vegetation Cover Frequency

In this study, the E_S and E_v values developed by (Sobrino et al., 2001) dalam **Table 2**.

Table 2. Emissivity Value

Emissivity	Band 10	Band 11
E_S	0.971	0.977
E_v	0.987	0.989

After that, the mean and difference values of the LSE are calculated through the equation:

$$m = \frac{LSE10 + LSE11}{2} \quad \text{.....(9)}$$

$$\Delta m = LSE10 - LSE11 \quad \text{.....(10)}$$

Description:
m = Mean of LSE
Δm = Difference of LSE
LSE10 = *Land Surface Emissivity* of Band 10
LSE11 = *Land Surface Emissivity* of Band 11

The final step involves calculating LST using the following equation.

$$LST = BT_{10} + C_1(BT_{10} - BT_{11}) + C_2(BT_{10} - BT_{11})^2 + C_{0+}(C_3 + C_4 W)(1 - m) + (C_5 + C_6)\Delta m \quad \text{.....(11)}$$

Description:
LST : Land Surface Temperature (°C)
BT10 : Brightness Temperature of Band 10 (°C)
BT11 : Brightness Temperature of Band 11 (°C)
Δm : Difference of LSE
m : Mean of LSE
W : Water Vapor Values (g/cm2)

The Split-Windows coefficient value (C) uses the values developed by (Sobrino et al., 2001) in the following **Table 3**.

Table 3. Split-Windows Coefficient Value

Coefficient	Value
C0	-0.268
C1	1.378
C2	0.183
C3	54.300
C4	-2.238
C5	-129.200
C6	16.400

2.2.4 Statistics Analysis

A. Normality Test
The normality test is carried out to test the normality of the distribution (pattern) of data by assuming that the data on each variable comes from a normally distributed population (Wulansari, 2018). This test is one of the requirements for parametric statistical testing with t test comparisons, ANOVA, product moment correlation, multiple correlation, simple linear regression analysis and multiple linear regression. This test is one of the requirements for parametric statistical testing with t test comparisons, ANOVA, product moment correlation, multiple correlation, simple linear regression analysis and multiple linear regression.

B. Homogenitas Homogeneity Test
The homogeneity test is carried out to test the difference in variance between two or more data groups by assuming that the data on each variable has a homogeneous variance with data on other variables (Wulansari, 2018). In addition to the normality test, this test is also a prerequisite for parametric statistical testing.

C. Regresi Linear Sederhana
Regression is a statistical method that discusses the logical relationship pattern between two or more variables where one variable is the dependent variable and the other variable is the independent variable (Wulansari, 2018). In the simple linear regression test, there is one dependent variable with one independent variable.

D. Binary (Dichotomous) Logistic Regression Test
Logistic regression test is a test applied to model the response variable (y) which is categorical based on one or more predictor variables (x), both categorical and continuous (Wulansari, 2023). While the binary (dichotomous) regression test is a model if the response variable (y) consists of 2 categories, namely y = 1 (success) and y = 0 (failure)

3. RESULTS AND DISCUSSION

3.1 Processing of LST Estimation

In this study, Land Surface Temperature (LST) was derived using Google Earth Engine (GEE) from multiple satellite datasets, including Landsat 8 Collection 2 Digital Number, Landsat 8 Collection 2 Surface Reflectance, and HLS-2 Landsat Operational Land Imager Surface Reflectance and TOA Brightness Daily Global (HLS-L30). The

specific processing methods applied to each dataset are detailed in **Table 4**.

Table 4. LST Processing Method

Satellite Datasets	Processing Method	
	MWA	SWA
Landsat 8 Collection 2 Digital Number	✓	✓
Landsat 8 Collection 2 Surface Reflectance	✓	×
HLS-L30	✓	✓

According to (Wang et al., 2019) the Mono Window Algorithm (MWA) developed (Qin et al., 2001) estimates Land Surface Temperature (LST) using a single thermal band, such as Band 10 from Landsat 8 TIRS. In the same study, the Split Window Algorithm (SWA), originally proposed by (McMillin, 1975), utilizes two thermal bands—typically Bands 10 and 11—to account for differences in atmospheric absorption and enhance LST accuracy. The selection of Band 10 is based on recommendations from the USGS (Landsat Missions, 2019) , which highlight its lower radiometric uncertainty and minimal influence from stray light compared to Band 11. This is supported by findings from (Galve et al., 2022) , which reported that Band 11 exhibits a greater positive bias (~0.2°K) relative to Band 10.

For each satellite dataset listed in Table 4, scenes with cloud cover less than or equal to 10% over the Mount Ungaran Geothermal Working Area (WKP) were selected. As a result, each satellite image type yielded a varying number of scenes, which were subsequently processed to generate LST products. The final LST outputs for each satellite dataset were derived through layer stacking operations, including mean, median, minimum, and maximum composites. Using the Mono Window Algorithm (MWA) and Split Window Algorithm (SWA), a total of 20 initial LST datasets were produced. Each of these datasets was further processed using 1×1 pixel focal statistics (mean, median, minimum, and maximum) to reduce spatial noise, resulting in 80 additional LST datasets. In total, these two processing steps yielded 100 LST products. Figure 3 illustrates this workflow using an example from the Landsat 8 Collection 2 Digital Number dataset processed with the MWA method for the year 2019.

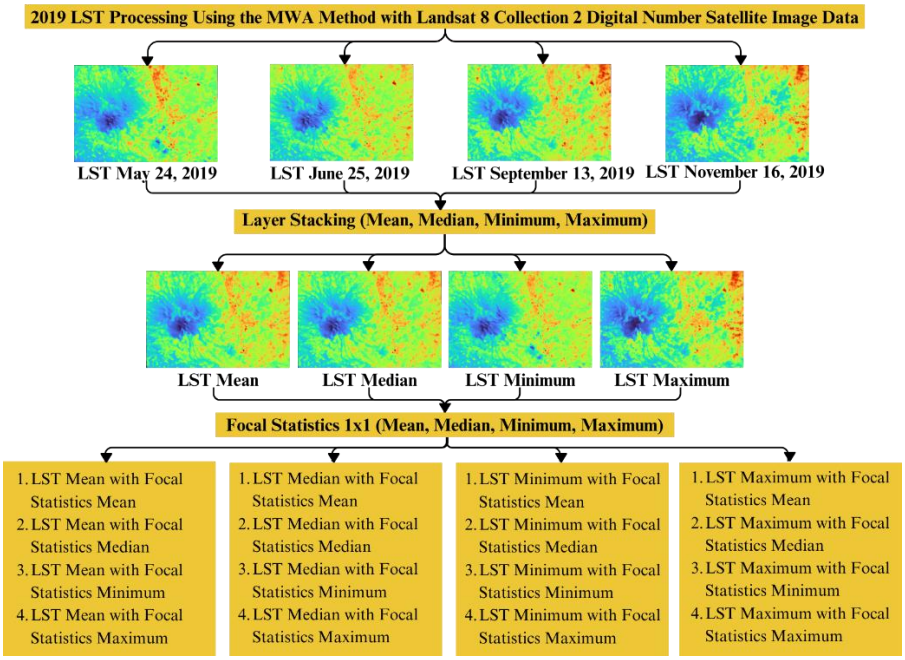

Figure 3. LST Processing Illustration

Each processed LST dataset underwent an extraction process based on the geographic coordinates of 18 known geothermal manifestation points. This resulted in LST values for all 18 points across the 100 processed LST datasets. The extracted LST data were then subjected to statistical analysis using Google Colab to identify the most appropriate LST estimation method for assessing geothermal potential.

3.2 Statistics Analysis

Parametric statistical tests such as simple linear regression analysis require prerequisites of normality and homogeneity tests. Therefore, to

determine the type of statistical test to be used (parametric or nonparametric), normality and homogeneity tests are conducted. Based on the results of these two tests, if the field temperature data and 100 LST data are not normally distributed and/or not homogeneous, then a non-parametric statistical test is performed, specifically the binary logistic regression test (dichotomous). However, if the distribution of all data is normal and the variance between field temperature and 100 LST data is homogeneous, then a parametric statistical test is performed, specifically the simple linear regression test. The following are the results of the statistical tests that have been conducted.

3.2.1. Normality Tests

In this study, normality testing was performed using the Shapiro-Wilk method to test the normality of the distribution (pattern) of field temperature data (sourced from PLN Geothermal) and 100 LST data at manifestation points. The reason for choosing the Shapiro-Wilk normality test method was because the number of sample points was ≤ 50. In this case, there were only 18 manifestation points as temperature sample points. The hypotheses in the normality test are:

H0: The data is normally distributed (p-value ≥ α)

H1: The data is not normally distributed (p-value < α)

The value of α is the significance level chosen, which is 0.05.

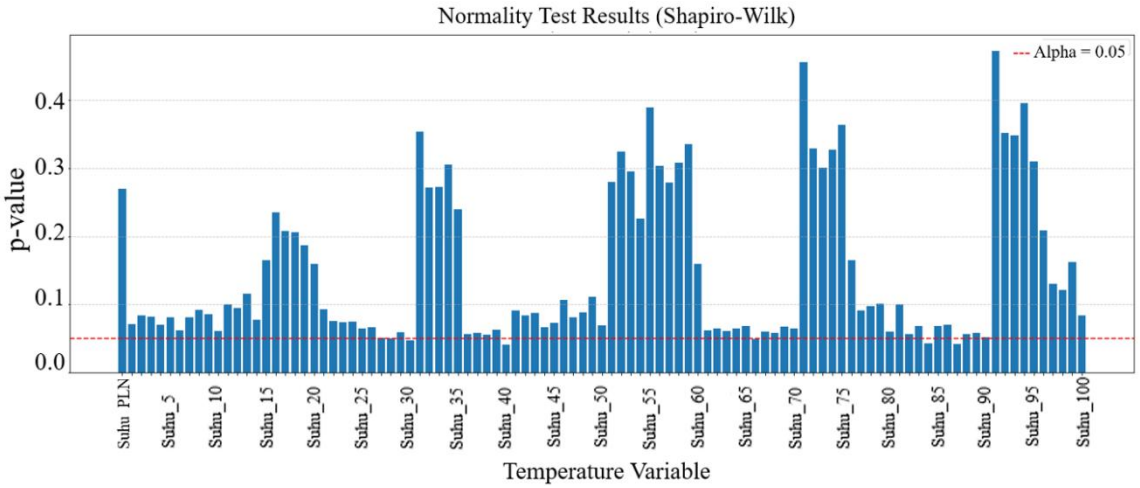

Figure 4. Normality Test Result Graph

Based on **Figure 4**, it is known that the p-value of the PLN temperature data and 96 LST data is ≥ 0.05. This value is greater than α, so H0 is accepted, namely that the PLN temperature and 96 LST data are normally distributed. In addition, it can be concluded that the majority of the data is around the average (there are no temperature values that spike up or down).

3.2.2. Homogeneity Tests

A homogeneity test was conducted to assess whether the PLN temperature data and each LST processed data had similar variances (homogeneous). In the homogeneity test, there were two hypotheses, namely:

H0: Data variance is homogeneous (p-value ≥ α)

H1: Data variance is not homogeneous (p-value < α)

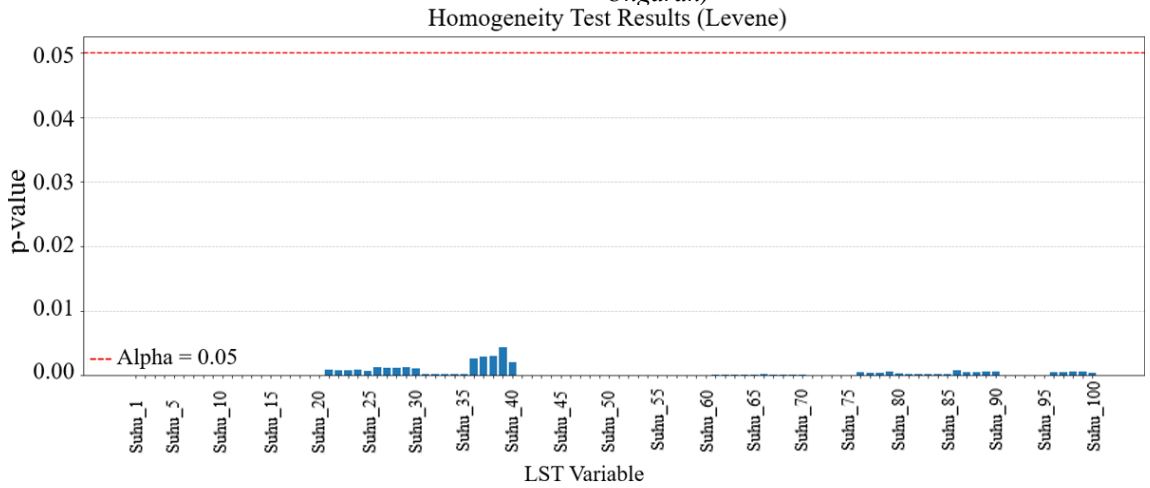

Figure 5. Homogeneity Test Result Graph

Based on the results of the homogeneity test shown in **Figure 5**, the p-value of each LST data is < 0.05, so it can be concluded that the variance between PLN temperature and 100 LST temperatures is not homogeneous (different).

3.2.3. Binary (Dichotomous) Logistic Regression Test

Based on the results of normality and homogeneity tests, four LST temperature datasets were found to have a normal distribution; however, none of them showed homogeneous variance when compared to field temperature (Suhu_PLN). Therefore, the assumptions required for parametric statistical tests were not fulfilled. Consequently, a non-parametric statistical approach, namely Binary Logistic Regression, was employed for further analysis.

The Binary Logistic Regression test was applied to evaluate the ability of each LST layer to distinguish geothermal manifestation points from non-manifestation (random) points. This method is appropriate because the dependent variable (test point category) is binary (1 = manifestation, 0 = non-manifestation), while the independent variable (LST temperature) is continuous. The analysis used 100 LST data points from 18 manifestation locations and 20 randomly selected non-manifestation points. The logistic regression model was developed to assess the influence of LST temperature on the probability that a location belongs to the manifestation category.

The hypotheses tested are as follows:

H0: The LST temperature variable has no significant effect on the test point category (p-value ≥ α)

H1: The LST temperature variable significantly affects the test point category (p-value < α).

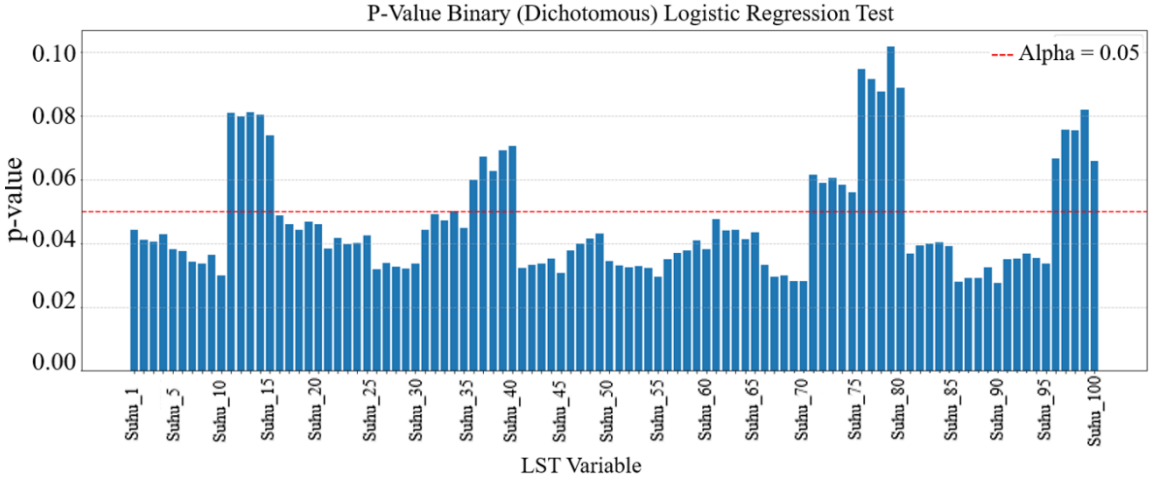

Figure 6. P-Value Graph of Binary Logistic Regression Test Results (Dichotomous)

As shown in **Figure 6**, 74 LST data points were found to have a significant influence (p-value < 0.05) on the classification between manifestation and non-manifestation points. In addition to the p-

value, the Pseudo R^2 value was used to indicate the strength of the relationship between the predictor variable (LST temperature) and the dependent variable (test point category). A higher Pseudo R^2 value represents a better model performance in explaining the variation in actual temperature and, consequently, higher statistical prediction accuracy. **Figure 7** illustrates that 100 LST temperature data can only explain about 6% to 11% of the data variation. Based on the p-value and Pseudo R2 values in **Figures 6 and 7**, Suhu_90 or the median LST from HLS-L30 processed using the Split Window Algorithm (SWA) with minimum Focal Statistics. was determined as the best model, with a p-value 0.028 and Pseudo $R^2 \approx 0.11$ or 11%.

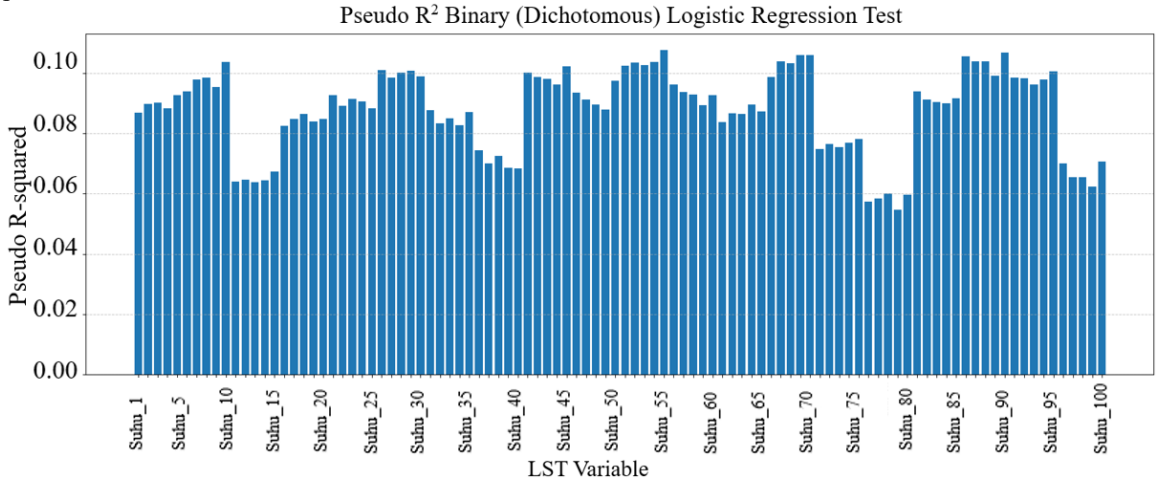

Gambar 7. Pseudo R^2 Graph of Binary Logistic Regression Test Results (Dichotomous)

The relatively low Pseudo R^2 values (6–11%) indicate that while LST temperature is statistically significant in differentiating geothermal manifestation points, it explains only a small proportion of the total variability in the data. This is expected in environmental modeling, particularly when using satellite-derived LST, as surface temperature is influenced by numerous factors such as land cover heterogeneity, atmospheric conditions, sensor spatial resolution, and temporal differences between image acquisition and field measurements. These uncontrolled factors contribute to random variations, reducing the model's explanatory power.

Despite the low Pseudo R^2 values, the HLS-L30 minimum SWA method was identified as the best-performing model because it produced the lowest p-value (0.028) and the highest Pseudo R^2 (0.11) among all tested models. The SWA approach effectively reduces atmospheric and emissivity-related errors by incorporating dual-band thermal information, while the use of minimum Focal Statistics minimizes the influence of extreme pixel values caused by noise or mixed land-cover conditions. Consequently, this method provides a more stable and representative estimation of ground temperature around geothermal manifestation areas. However, it is important to note that this method was tested only within the WKP Mount Ungaran area, and has not yet been validated in other geothermal fields. Therefore, it is strongly recommended to reprocess the data and repeat the analysis from the beginning when applying this approach to other study areas. Differences in local surface characteristics, atmospheric conditions, and geothermal manifestations may affect the model's performance and lead to variations in accuracy and statistical significance.

Figure 8 presents the spatial distribution of the 2019 LST over the WKP Mount Ungaran area derived from the best-performing model, i.e., the median LST of HLS-L30 using the SWA method with minimum Focal Statistics.

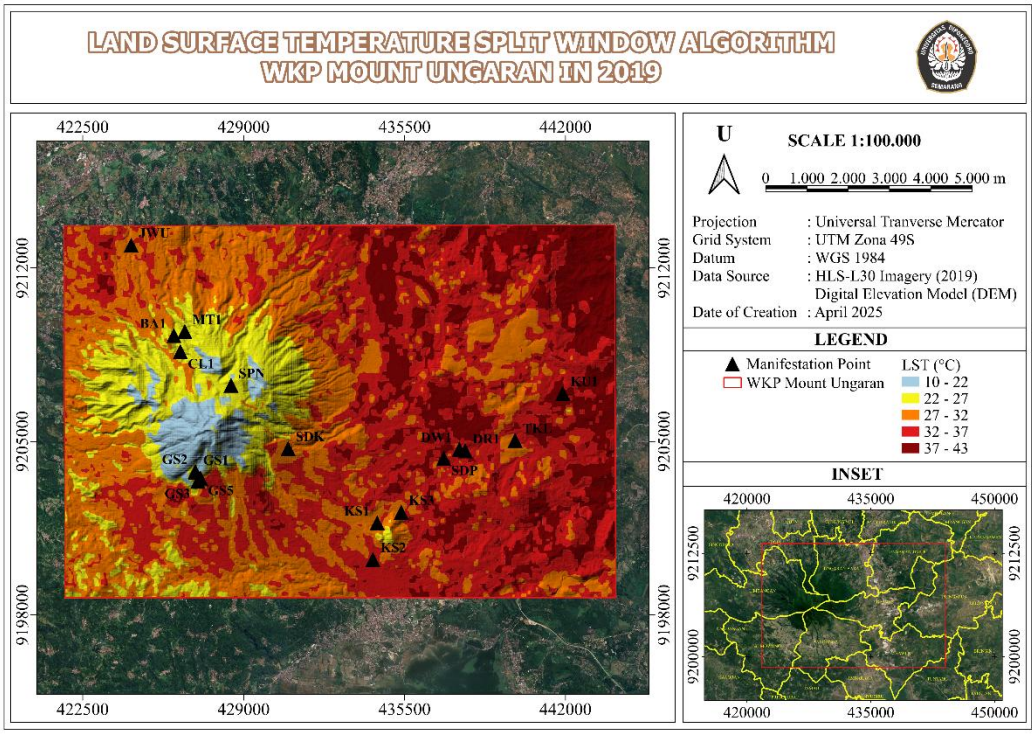

Figure 8. Final LST 2019 WKP Mount Ungaran

The results of LST extraction and field temperature (PT PLN Gas & Geothermal) at 18 manifestation points of the WKP Mount Ungaran can be seen in **Table 5**.

Table 5. LST and Field Temperature at 18 Manifestation Points

Manifestation Points	LST (°C)	Field Temperature (°C)
BA1	25.427	33.200
KS1	31.223	29.700
KS2	32.397	36.300
KS3	30.270	54.500
GS1	25.427	39.300
GS2	25.427	43.200
GS5	26.195	50.800
DW1	32.120	35.900
DR1	32.142	45.300
KU1	38.979	39.400
MT1	24.929	27.100
SDP	38.816	20.400
SPN	28.216	20.000
CL1	25.015	27.400
TKL	35.121	18.200
SDK	31.630	21.600
GS3	24.380	22.100
JWU	29.978	23.000

Table 5 indicates that at several manifestation points, there are notable discrepancies between the LST data and the field temperature data obtained from PLN. One possible explanation is that, although cloud cover was filtered to ≤ 10%, the satellite imagery may still contain residual cloud presence, which can affect the accuracy of LST processing. Additionally, some manifestation points are located in or near areas of dense vegetation. In such cases, the satellite detects the surface temperature of the vegetation canopy rather than the actual ground surface temperature of the geothermal manifestation point.

This is supported by findings from (Alqahtani et al., 2023), who reported a negative correlation between LST and NDVI, with correlation coefficients ranging from -0.28 to -0.53. These results suggest that areas with dense vegetation typically exhibit lower surface temperatures, reinforcing the idea that vegetation can obscure or "mask" geothermal surface anomalies when using satellite-derived LST.

4. CONCLUSION

Based on the analysis results, 74 out of 100 LST data points were correctly classified into geothermal manifestation and non-manifestation categories. The model showed statistical significance ($p = 0.037$) but limited explanatory power (Pseudo $R^2 \approx 10\%$). Among all datasets, the HLS-L30 imagery processed with the Split Window Algorithm (SWA) using minimum focal statistics performed best ($p = 0.028$; Pseudo $R^2 \approx 0.11$). However, the low Pseudo R^2 values (6–11%) indicate that surface temperature

is affected by environmental and technical factors such as land cover, atmosphere, and resolution differences.

The selected HLS-L30 SWA method with minimum focal statistics is valid only for the Mount Ungaran area and should not be generalized without recalibration. Overall, satellite-based LST analysis using HLS-L30 SWA shows good potential for supporting geothermal exploration. Future studies are encouraged to include additional parameters and test the method in other geothermal regions to improve model accuracy.

REFERENCES

Akhyar, & Sary, C. A. (2024). Identification of geothermal potential zone associated with land surface temperature derived from Landsat 8 data using split-window algorithm. *Journal of Applied Research and Technology*, *22*(June), 125–137. https://doi.org/10.22201/icat.24486736e.2024.22.1.2091

Alqahtani, F., Aboud, E., Ehsan, M., Naseer, Z., Abdulfarraj, M., Abdelwahed, M. F., & El-Masry, N. (2023). Geothermal Exploration Using Remote Sensing, Surface Temperature, and Geophysical Data in Lunayyir Volcanic Field, Saudi Arabia. *Sustainability (Switzerland)*, *15*(9), 1–21. https://doi.org/10.3390/su15097645

Dinas Energi dan Sumber Daya Mineral Provinsi Jawa Tengah. (2022). *Potensi Panas Bumi di Jawa Tengah*. https://data.jatengprov.go.id/dataset/potensi-panas-bumi-di-jawa-tengah

Engebretson, C. (2020). Landsat 8-9 Operational Land Imager (OLI) - Thermal Infrared Sensor (TIRS) Collection 2 Level 1 (L1) Data Format Control Book (DFCB). In *Department of the Interior U.S. Geological Survey* (Vol. 2, Issue September). https://prd-wret.s3.us-west-2.amazonaws.com/assets/palladium/production/atoms/files/LSDS-1822_Landsat8-9-OLI-TIRS-C2-L1-DFCB-v6.pdf

Galve, J. M., Sánchez, J. M., García-Santos, V., González-Piqueras, J., Calera, A., & Villodre, J. (2022). Assessment of Land Surface Temperature Estimates from Landsat 8-TIRS in A High-Contrast Semiarid Agroecosystem. Algorithms Intercomparison. *Remote Sensing*, *14*(8). https://doi.org/10.3390/rs14081843

Izzatinavia, A., Yulianto, T., & Nurwidyanto, M. I. (2024). Geothermal Prospect Zone Estimation Based on Landsat 8 Satellite Imagery (Case Study Around Gedongsongo). *International Journal of Research and Review*, *11*(6), 68–78. https://doi.org/10.52403/ijrr.20240609

Ju, J., Neigh, C., Claverie, M., Skakun, S., Roger, J., Vermote, E., & Dungan, J. (2023). *Harmonized Landsat Sentinel-2 (HLS) Product User Guide* (Vol. 2). https://lpdaac.usgs.gov/documents/1698/HLS_User_Guide_V2.pdf

Kementerian Energi dan Sumber Daya Mineral. (2013). *Menteri ESDM : Malu Saya, 40% Geothermal Dunia Ada Di Indonesia Namun Yang Baru Dikembangkan 4% Saja*. Kementerian Enerdi Dan Sumber Daya Mineral Republik Indonesia. https://www.esdm.go.id/id/media-center/arsip-berita/menteri-esdm-malu-saya-40-geothermal-dunia-ada-di-indonesia-namun-yang-baru-dikembangkan-4-saja

Kementerian Energi dan Sumber Daya Mineral Republik Indonesia. (2007). *Keputusan Menteri ESDM No. 1789 K/33/MEM/2007 Tentang Penetapan Wilayah Kerja Pertambangan Panas Bumi Di Daerah Gunung Ungaran, Kabupaten Semarang Dan Kabupaten Kendal, Provinsi Jawa Tengah*. Keputusan Menteri ESDM No. 1789 K/33/MEM/2007 Tentang Penetapan Wilayah Kerja Pertambangan Panas Bumi Di Daerah Gunung Ungaran, Kabupaten Semarang Dan Kabupaten Kendal, Provinsi Jawa Tengah

Landsat Missions. (1984). *Using the USGS Landsat Level-1 Data Product*. USGS. https://www.usgs.gov/landsat-missions/using-usgs-landsat-level-1-data-product

Landsat Missions. (2019). *Landsat 8 OLI and TIRS Calibration Notices*. USGS. https://www.usgs.gov/landsat-missions/landsat-8-oli-and-tirs-calibration-notices

McMillin, L. M. (1975). Estimation of Sea Surface Temperatures from Two Infrared Window Measurements with Different Absorption. *Journal of Geophysical Research*. https://doi.org/https://doi.org/10.1029/JC080i036p05113

Mirwanda, S., Salsabila, F., Pramesti, R., Zakiyyah,

A. R., & Tuelzar, M. R. (2021). Pemetaan Suhu Permukaan Anomali Panas Bumi Daerah Gunung Ciremai Menggunakan Data Inframerah Termal Landsat 8. *Jurnal Geosains Dan Remote Sensing*, *2*(2), 92–99. https://doi.org/10.23960/jgrs.2021.v2i2.64

Pambudi, N. A., Yuniar, W., Ulfa, D. K., Nanda, I. R., & Widiastuti, I. (2024). Assessing the Readability of Renewable Energy Education Material from Geothermal Resources in Vocational High School Textbooks: A Case Study in Indonesia. *Journal of Sustainable Development of Energy, Water and Environment Systems*, *12*(3). https://doi.org/http://dx.doi.org/10.13044/j.sdewes.d12.0506

Qin, Z., Karnieli, A., & Berliner, P. (2001). A mono-window algorithm for retrieving land surface temperature from Landsat TM data and its application to the Israel-Egypt border region. *International Journal of Remote Sensing*, *22*(18), 3719–3746. https://doi.org/10.1080/01431160010006971

Ramadhan, R. F., & Saputra, R. A. (2021). Identifikasi Area Prospek Panas Bumi Menggunakan Integrasi Citra Landsat 8 OLI/TIRS dan DEM : Studi Kasus Batu Bini, Kalimantan Selatan. *Majalah Ilmiah Swara Patra*, *11*(2), 37–50. https://doi.org/10.37525/sp/2021-2/294

Ramadhani, A. B., & Hidayat, H. (2021). Analisis Pemetaan Potensi Panas Bumi dengan Menggunakan Penginderaan Jauh (Studi Kasus: Kecamatan Hu'u Kabupaten Dompu, Nusa Tenggara Barat. *Jurnal Teknik ITS*. https://repository.its.ac.id/87388/

Sobrino, J. A., Reillo, S., Laporta, S., & Cuenca, J. (2001). Algorithms for Estimating Surface Temperature from ATSR-2 Data. *Remote Sensing for Agriculture, Ecosystems, and Hydrology II*, *4171*(December), 249–260. https://doi.org/10.1117/12.413933

Utama, P. P., Yoni, D. R., Amalia, D., Ulhaq, I. D., & Arya, M. S. F. (2024). Geothermal potential area analysis using Landsat 8 OLI/TIRS and digital elevation model images (case study: Lawu Mount, Central Java). *IOP Conference Series: Earth and Environmental Science*, *1339*(1). https://doi.org/10.1088/1755-1315/1339/1/012004

Wang, L., Lu, Y., & Yao, Y. (2019). Comparison of three algorithms for the retrieval of land surface temperature from landsat 8 images. *Sensors (Switzerland)*, *19*(22). https://doi.org/10.3390/s19225049

Wulansari, A. D. (2018). Aplikasi Statistika Parametrik dalam Penelitian. In R. Widyaningrum (Ed.), *Pustaka Felicha* (III). Pustaka Felicha. https://repository.iainponorogo.ac.id/1391/1/Buku Aplikasi Statistika Parametrik dalam Penelitian.pdf

Wulansari, A. D. (2023). *Aplikasi Statistika Nonparametrik dalam Penelitian* (K. Hidayati (ed.); I). Pustaka Felicha. https://repository.iainponorogo.ac.id/1526/1/Aplikasi Statistika Nonparametrik dalam Penelitian Rev3.pdf

Yanis, M., Zaini, N., Novari, I., Abdullah, F., Dewanto, B. G., Isa, M., Marwan, Zainal, M., & Abdurrahman. (2023). Monitoring of Heat Flux Energy in the Northernmost Part of Sumatra Volcano Using Landsat 8 and Meteorological Data. *International Journal of Renewable Energy Development*, *12*(1), 55–65. https://doi.org/10.14710/ijred.2023.47048